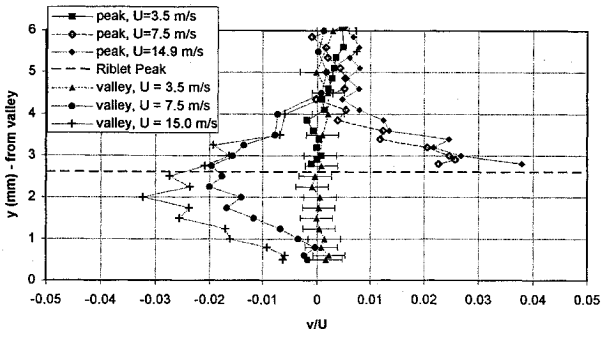

Fig. 2 Peak and valley v/U profiles, x = 300 mm.

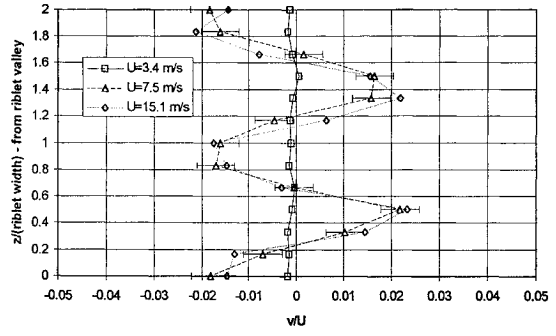

Fig. 3 Spanwise v-velocity profiles, y = 0.5 mm above peak, x = 300 mm.

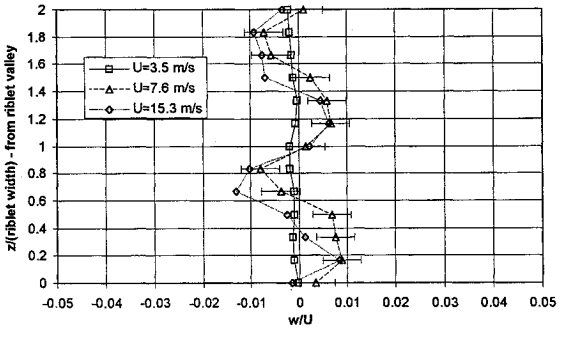

Fig. 4 Spanwise w-velocity profiles, y = 0.5 mm above peak, x = 300 mm.

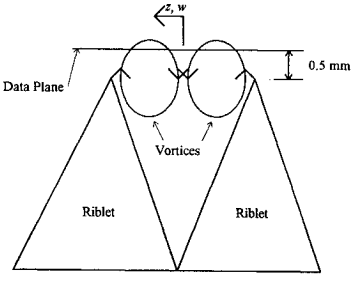

Fig. 5 Sketch of vortices within riblet valley.

above the peaks. The z parameter is the spanwise distance divided by the riblet spacing, with the datum directly over a riblet valley. Figure 3 shows a spanwise periodic pattern of ascending and descending particles just above the riblets. Paired vortical motion is confirmed in Fig. 4, which shows spanwise periodic patterns of alternating w velocities, with wavelength equal to the riblet spacing and offset in phase from the v profiles by 90 deg. The signs of the w velocities indicate that the vortex cores lie below the plane of data acquisition, as illustrated in Fig. 5. There was no significant vortical motion for the low speed case at x = 300 mm.

An inspection of all data obtained reveals that the vertical velocity component v was detected before (<100 mm upstream of) the spanwise component w, and both components are always $\lesssim$4% of the freestream velocity. Once formed, the vortices appear to maintain a constant position within the riblet profile. Finally, in the fully turbulent region for $U \cong$ 7.5 and 15.0 m/s, the maximum v/U and w/U components were similar in magnitude and approximately equal to 0.04.

Conclusions

Three-dimensional measurements of air velocity within and above riblets indicate the evolution of counter-rotating pairs of vortices during transition to turbulent flow. These vortices extend slightly above the riblet peaks and, once fully developed, maintain a constant location within the riblet profile with component velocities up to 4% of the freestream velocity. The vortices remain intact and of constant size downstream into the fully turbulent boundary-layer region.

References

[1]Walsh, M. J., "Riblets," *Viscous Drag Reduction in Boundary Layers*, edited by D. M. Bushnell and J. N. Heffner, Vol. 123, Progress in Astronautics and Aeronautics, AIAA, Washington, DC, 1990, pp. 203–261.

[2]Choi, K.-S., "Near Wall Structure of a Turbulent Boundary Layer with Riblets," *Journal of Fluid Mechanics*, Vol. 208, Nov. 1989, pp. 417–458.

[3]Suzuki, Y., and Kasagi, N., "Turbulent Drag Reduction Mechanism Above Riblet Surface," *AIAA Journal*, Vol. 32, No. 9, 1994, pp. 1781–1790.

[4]Schlichting, H., *Boundary Layer Theory*, 7th ed., McGraw–Hill, New York, 1979, p. 480.

Magnitude of Artificial Dissipation for Numerical Simulations

Y. Kallinderis* and H. McMorris†
University of Texas at Austin, Austin, Texas 78712

I. Introduction

A COMMON method for stabilizing numerical solutions is the addition of artificial dissipation. It is employed in order to suppress solution oscillations, as well as to capture shock waves with central-differencing numerical schemes.[1] This is usually achieved via a combination of second and fourth differences. The former is employed for shock capturing, whereas the latter is used for suppression of the odd-even modes of the numerical solution.[2] The amount of smoothing depends on ad hoc coefficients that are chosen a priori and remain the same during the computation. Artificial dissipation frequently results in severe deterioration of numerical accuracy, and especially so in cases of viscous flow simulations. Contamination of boundary-layer profiles due to smoothing is quite common.[3]

A simple method is proposed in the present work in order to calculate specific values of the smoothing coefficient that also result in a bounded amount of dissipation. The main differences with the classical approach of explicit smoothing are 1) the values of the smoothing coefficient are calculated and not chosen a priori, 2) the magnitude of artificial dissipation is bounded, 3) the values change dynamically during the computation, 4) separate values are employed for each one of the governing equations, and 5) the values can change spatially instead of the same value being employed everywhere in the computational domain.

Received Aug. 8, 1994; revision received Dec. 14, 1994; accepted for publication Dec. 22, 1994.

*Associate Professor, Department of Aerospace Engineering and Engineering Mechanics. Member AIAA.

†Undergraduate Research Assistant, Department of Aerospace Engineering and Engineering Mechanics.

The scheme used for the study is a typical finite volume, central-differencing method with Lax–Wendroff time marching. The cases considered include both inviscid and viscous simulations with and without shock waves.

II. Calculation of the Amount of Dissipation

A. Finite Volume Method

The Navier–Stokes system may be written in Cartesian two-dimensional conservation form as

$$\frac{\partial \boldsymbol{U}}{\partial t} + \frac{\partial (\boldsymbol{F}_I - \boldsymbol{F}_V)}{\partial x} + \frac{\partial (\boldsymbol{G}_I - \boldsymbol{G}_V)}{\partial y} = 0 \tag{1}$$

In Eq. (1) $\boldsymbol{U}$ is the state vector comprising the variables of density, the two components of momentum and the total energy. The vectors $\boldsymbol{F}_I$ and $\boldsymbol{G}_I$ represent the convective terms, and $\boldsymbol{F}_V$ and $\boldsymbol{G}_V$ are the vectors corresponding to the diffusion terms.

The two-dimensional Navier–Stokes equations are integrated over an area S, and the surface integrals are evaluated using Green's theorem, which results in the following:

$$\frac{\partial}{\partial t}\int\int_S \boldsymbol{U}\,\mathrm{d}S + \oint_{\partial S} [(\boldsymbol{F}_I - \boldsymbol{F}_V)\,\mathrm{d}y - (\boldsymbol{G}_I - \boldsymbol{G}_V)\,\mathrm{d}x] = 0 \tag{2}$$

The discrete form of the previous equation is

$$\delta \boldsymbol{U} = -\frac{\Delta t}{\Delta S}\sum_{\text{cell}} [(\boldsymbol{F}_I - \boldsymbol{F}_V)\Delta y - (\boldsymbol{G}_I - \boldsymbol{G}_V)\Delta x] \tag{3}$$

where $\delta \boldsymbol{U}$ denotes the change in time $(\boldsymbol{U}^{n+1} - \boldsymbol{U}^n)$ of the state vector $\boldsymbol{U}$, ΔS is the area of each computational cell, and Δx and Δy are the projections of the edges of the cell in the x and y directions.

A typical formulation of the combined second- and fourth-order smoothing operator is

$$\delta \boldsymbol{U}^S = \sigma_2 S_2 \Delta_{xx} \boldsymbol{U} - \sigma_4 S_4 \Delta_{xxxx} \boldsymbol{U} \tag{4}$$

where σ_2 and σ_4 are constant coefficients. The terms S_2 and S_4 are suitable switches for limiting the second-order dissipation in the vicinity of shock waves and for keeping the fourth-order smoothing elsewhere.[2] Lastly, $\Delta_{xx}\boldsymbol{U}$, $\Delta_{xxxx}\boldsymbol{U}$ denote second- and fourth-order spatial differences of the solution. In the expression for artificial dissipation the constants σ_2 and σ_4 control the level of smoothing. In the past, they have been chosen empirically via trial and error procedures. They are constant throughout the computational domain, as well as during the time-marching process. Such trial and error procedures are usually limited to the specific case being simulated and do not guarantee low levels of dissipation when different cases are computed.

B. Specified Ratio of Artificial Dissipation to Convection Diffusion

The proposed method for determining values for the smoothing coefficients is based on the principle of limiting the magnitude of the smoothing contribution $\delta \boldsymbol{U}^S$ to be a certain percentage of the contribution of the real convective and viscous term $\delta \boldsymbol{U}$. The values are adjusted during time marching since so that the magnitude of artificial dissipation is bounded and it remains a certain fraction of the magnitude of the convective and viscous terms. This is achieved by specifying the ratio R of these terms as follows:

$$R = \frac{|\delta \boldsymbol{U}^S|}{|\delta \boldsymbol{U}|} = \frac{|\sigma_4 S_4 \Delta_{xxxx} \boldsymbol{U}|}{|\delta \boldsymbol{U}|} \tag{5}$$

which yields the following expression for the smoothing coefficient:

$$\sigma_4 S_4 = R\frac{|\delta \boldsymbol{U}|}{|\Delta_{xxxx}\boldsymbol{U}| + \epsilon} \tag{6}$$

The switch S_4 is included in order to cover cases with shock waves for which it is used to limit fourth-order smoothing away from shock waves. It is more plausible to specify a value for the ratio R than it is to assign a value to σ_4. The term ϵ is a small number added to the denominator in order to avoid indeterminancy in cases in which $\Delta_{xxxx}\boldsymbol{U} = 0$. Separate values of the coefficient σ_4 are used for each one of the governing equations. The ratio is not the ratio of the actual smoothing error, since $\delta \boldsymbol{U}$ is not the exact solution. However, the relation does limit the magnitude of the smoothing operator to be a small percentage of the magnitude of the real term during each time step independently from the form of the numerical solution. Furthermore, the present method causes a reduction in the amount of artificial dissipation as steady state is approached, since $\delta \boldsymbol{U}$ goes to zero. In cases in which shock waves are not present, $S_4 = 1$ in Eq. (6). The method is employed for fourth-order dissipation. Second-order smoothing is used to capture shock waves and should be negligible elsewhere. At the vicinity of shocks $\delta \boldsymbol{U}^S$ is the dominant term, and a similar relation to Eq. (6) cannot be used.

The terms $\delta \boldsymbol{U}$ and $\delta \boldsymbol{U}^S$ vary throughout the domain and, therefore, a separate value of the smoothing coefficient can be calculated for each computational element. In the present work, two approaches have been examined: 1) use of local values of the coefficient for each time-step and 2) computation of a single value of the coefficient to be used everywhere in the domain at each time-step (global coefficient). The average value over the entire domain has been employed for that purpose. Other candidates are the minimum and maximum values of the coefficient. Such values are frequently not representative, however, since the smoothing operator stencil is usually incomplete at the boundaries resulting in artificial maxima and minima.

Examining Eq. (6), the following singular cases may occur: 1) $\Delta \boldsymbol{U}$ may be zero or very close to zero (e.g., initial marching steps, approach to steady state), and 2) $\Delta_{xxxx}\boldsymbol{U}$ may be zero (e.g., areas of uniform flow). The first case will result in very small value of $\sigma_4 S_4$, whereas the second case will yield a very large value of the term. In order to avoid these cases of singular behavior, upper and lower bounds are set for the values of the coefficient.

III. Numerical Tests

The test cases that are employed have been designed to examine the following issues: 1) the effect of different values of the ratio R on the fourth-order smoothing coefficient σ_4, 2) global vs local values of the smoothing coefficient, 3) the behavior of the artificial dissipation coefficient with and without shock waves, and 4) behavior of the coefficient for both inviscid and viscous cases. The inviscid (Euler) cases include attenuation of a perturbation in density of stagnant fluid, as well as subsonic and transonic flow around a circular bump in a channel. The viscous (Navier–Stokes) cases consider flat plate flow (Blasius boundary layer).

An initially stagnant fluid is perturbed by raising the density by 10% at a point in the interior. The steady-state solution was stagnant fluid. The evolution of the fourth-order smoothing coefficient σ_4 during the computation of the attenuating perturbation is illustrated in Fig. 1. It is observed that the value of the coefficient peaks and then reduces leveling off as steady state is approached. The values for each of the four equations are very close to each other. The lower curves A correspond to a specified ratio $R = 5\%$, whereas the upper curves B correspond to a higher value $R = 20\%$. It is observed that the values of σ_4 vary in proportion to the specified ratio. The values of the coefficient vary considerably for each equation in the case of subsonic flow over a circular bump with Mach number equal to 0.5. Figure 2 shows the evolution of the coefficient σ_4 for each one of the governing equations. Similarly to the previous case of the attenuating perturbation, the values peak and then reduce to a low level toward steady state. The same case was run without any artificial dissipation and yielded essentially the same result as the previous case of dynamically changing σ_4. The transonic flow case over the same bump with Mach number equal to 0.675 was also tested. The evolution of the term $\sigma_4 S_4$ was similar to the one observed in the previous subsonic case.

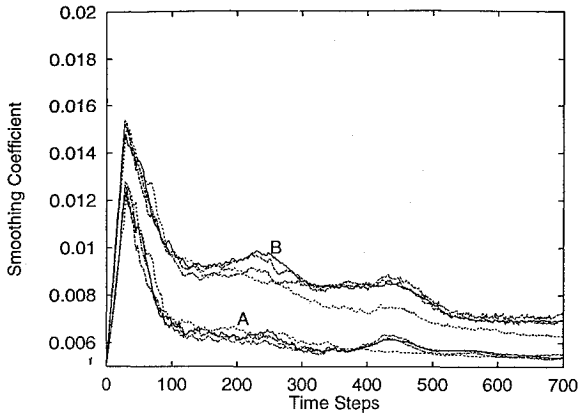

Fig. 1 Evolution of the smoothing coefficient σ_4 with time for each one of the four governing equations, case of attenuation of a perturbation in density of a stagnant inviscid fluid, curves A, R = 5%, and curves B, R = 20%; —, continuity; —·—, x momentum; - - -, y momentum; and — —, energy.

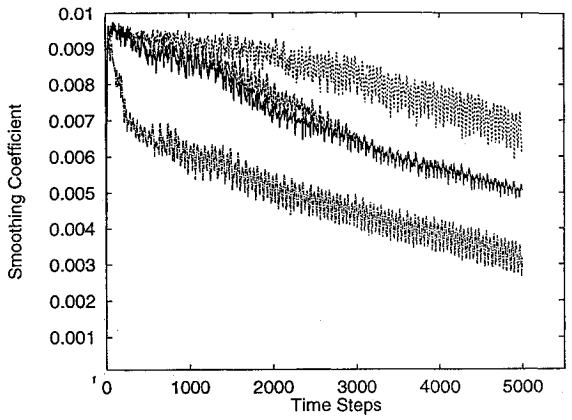

Fig. 2 Evolution of the smoothing coefficient σ_4 with time for each one of the four governing equations, case of subsonic inviscid flow over a circular bump with Mach number equal to 0.5: —, continuity; —·—, x momentum; - - -, y momentum; and — —, energy.

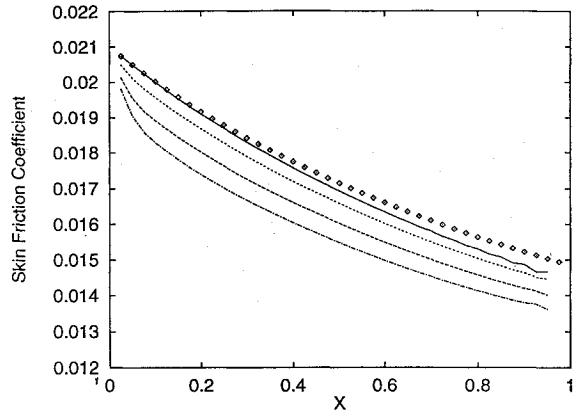

Fig. 3 Effect of ratio R on solution accuracy, comparison of skin friction distributions along a plate for Blasius boundary layer with $Re = 10^3$ with vertical scale enlarged: ◇, Blasius analytical solution; —, R = 0%; - - -, R = 5%; — —, R = 20%; —·—, $\sigma_4 = 10^{-3}$.

The case of Blasius flat plate flow is considered next. The Reynolds number is 10^3. Accuracy of the numerical solution is examined via comparisons of the skin-friction distribution with that of the analytical Blasius solution. Unlike the previous inviscid flow cases, the solution and especially the skin-friction values are very sensitive to the amount of artificial dissipation used. Different values of the ratio are prescribed which keep the magnitude of the smoothing term to be a certain percentage of the magnitude of the real convection-diffusion term. Figure 3 compares the numerical skin friction distributions to those given by the analytical Blasius result for values of R equal to 0%, 5%, and 20%. It is observed that increase in R results in proportional deterioration of numerical accuracy. The ratio R appears to be a quite accurate measure of the actual error in the numerical solution. Figure 3 also shows the distribution obtained via the classical approach of specifying a priori a constant value of σ_4 equal to 10^{-3}. It is observed that the result is less accurate than the one obtained with the present method using $R = 20\%$.

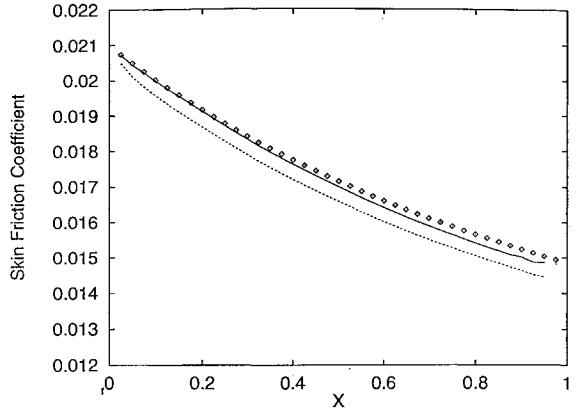

Fig. 4 Global vs local smoothing coefficient σ_4 with R = 5%, comparison of skin friction distributions along a plate for Blasius boundary layer with $Re = 10^3$ with vertical scale enlarged: ◇, Blasius analytical solution; —, spatially varying σ_4 (local); and - - -, spatially constant σ_4 (global).

The previous cases have employed the same value of the smoothing coefficient throughout the domain (global coefficient). The average value over all computational elements has been chosen. The next case uses the local values for σ_4 that are calculated via Eq. (6). Figure 4 compares the skin friction distributions yielded by the global as well as the local smoothing coefficients for the same value of the ratio R equal to 5%. It is observed that use of locally varying smoothing coefficients yielded a converged result with superior accuracy over the global coefficient.

IV. Concluding Remarks

Specification of the ratio of the magnitudes of allowed artificial dissipation to convection diffusion yielded bounded values of the smoothing coefficient that exhibited the same evolution in time for all cases considered. Dynamic change in the coefficient value with time step did not inhibit convergence to steady state even in the case of locally varying coefficients. The Blasius case showed that the ratio R appears to be a quite accurate measure of the actual error in the numerical solution. A direct relation between the value of R and the magnitude of the solution error was observed. The presented method is not limited to finite volume schemes. It is directly applicable to finite difference and to finite element methods, as well. Also, use of the ratio R is the same in both two and three dimensions.

Acknowledgments

This work was supported by National Science Foundation Grant ASC-9357677 (NYI program), as well as by Texas Advanced Technology Program (ATP) No. 003658-413.

References

[1]Pulliam, T. H., "Artificial Dissipation Models for the Euler Equations," AIAA Paper 85-0438, Jan. 1985.

[2]Jameson, A., Schmidt, W., and Turkel, E., "Numerical Solutions of the Euler Equations by Finite-Volume Methods Using Runge–Kutta Time-Stepping Schemes," AIAA Paper 81-1259, July 1981.

[3]Kallinderis, Y., "A Finite Volume Navier–Stokes Algorithm for Adaptive Grids," *International Journal for Numerical Methods in Fluids*, Vol. 15, No. 2, 1992, pp. 193–217.

New Method for the Eduction of Natural Coherent Structures

S. Aydöre* and P. J. Disimile†
University of Cincinnati, Cincinnati, Ohio 45221

Introduction

NATURAL large-scale coherent structure eduction is generally known to be troublesome. Even though these large-scale structures are repetitive, they are difficult to educe due to jitter and the natural variations in the structure shape, size, orientation, passage time, and trajectory.[1–3] Earlier these structures were studied using artificial excitation (acoustical, mechanical, etc.). It was assumed that the excited structures were approximately the same as the natural ones if low-level excitation were used.[2,4]

Conditional sampling techniques have been used extensively in the measurement of the coherent structures in the shear flows with or without external excitation.[2,4,5] In this technique, a reference probe is fixed in space and used for detection of coherent structure passage while a measurement probe is moved in space. Utilizing the information from the reference probe, quantitative data are often phase averaged to reveal the deterministic structure properties. One phase-averaging method used for eduction is the pattern recognition method. This method is based on the alignment of the events using amplitude, slope, and intermittencies. This method is believed to limit the selection and artificially modify the extracted pattern.

In order to educe the structures in an axisymmetric freejet, Zaman and Hussain[4] used several triggering criteria. They investigated the effects of the threshold level, triggering window, joint probability of longitudinal and lateral instantaneous signals, reference probe location, etc. on education. Their conclusion, "triggering on the positive peaks of the longitudinal velocity signal derived from the high speed side of the mixing layer," gave the best education. According to Bruun,[3] triggering on the high-speed-side peaks of the reference signal also obtained good results. However, when the peak amplitude of the longitudinal velocity signal is small, as in the current case, i.e., flows with fully turbulent pipe flow exit conditions, a better method was desired.[6]

Experimental Arrangement

In the present study, air was introduced into a circular delivery tube 45 diameters long with an inner diam of 5.08 cm. The jet was then allowed to impinge vertically onto a flat plate. All flowfield measurements were acquired with an X-wire, while a reference probe, a straight wire, was used to detect the coherent structure passage. Hot wires were sampled simultaneously at 2 kHz.

The Reynolds number based on the jet diameter D was 13,000, and the jet to plate spacing was $4D$. The measurement plane was formed by the jet centerline and the radial direction. There were 330 grid points in the measurement plane (30 streamwise and 11 radial R). After extensive fast Fourier transform (FFT) surveys, the reference wire was placed at $X/D = 1.0$ and $R/D = 0.25$. To minimize reference probe interference, the X wire was positioned on the jet's opposite side.

Received Jan. 25, 1993; revision received Jan. 17, 1995; accepted for publication Feb. 14, 1995.

*Graduate Student, Department of Aerospace Engineering and Engineering Mechanics; currently Assistant Professor, Istanbul Technical University, Aeronautical Engineering Department, Maslak 80626, Istanbul, Turkey.

†Bradley Jones Associate Professor, Department of Aerospace Engineering and Engineering Mechanics, M.L. 70. Member AIAA.

Life Cycle Method

After careful conditional sampling (structure identification and selection) phase averaging is employed by means of structure phase alignment. The time average of the reference signal is used to establish the threshold level for both triggering and cycle determination. Using this average value, the reference wire time series is interrogated. When the reference signal experiences a positive, traveling across the threshold level, that location in the time series is marked as the beginning of a cycle (Fig. 1). The end of the cycle is determined when the reference signal makes a second positive going across. This establishes the beginning and end of each cycle in the time series. Likewise, the corresponding X-wire time series is also marked and saved as a cycle.

Once a cycle is established the number of data points in the cycle is determined. If the number of data or phase points in a cycle is within the predetermined range $(M \pm N)$, then the cycle is accepted for future phase averaging. Here, M is a measure of the structure time scale (life time) and N determines the tolerance above and below a chosen scale. So there are M phase points in the phase-averaged cycle. Depending on the size of vortical structures that are intended to be educed, values of M and N are selected. A sample of such a histogram is presented in Fig. 2. As seen from the histogram, if the number of phase points in a cycle is very large (i.e., very large structures) only a limited number of the total population of vortical motions in the flowfield would be represented. Similarly, choosing short cycles would only enable the eduction of the smaller vortical structures. The present goal was to educe typical large-scale vortical structures. That is, those structures whose period, as determined from an FFT of the reference wire signal, was approximated to be 12.5 ms.

Preparing for phase averaging, normalization of the cycles is needed (Fig. 3). Normalization is achieved by nondimensionalization of the cycle by its period. This is referred to as phase alignment. Cycles which have less than M data points can be stretched, and cycles with more than M data points are compressed.

Several cases for various M and N values were evaluated for the current experimental data. Because of space considerations only two cases are presented: 1) $M = 30$ and $N = 7$ and 2) $M = 20$ and $N = 7$. An examination of the histogram indicates that these two cases account for 23% and 33%, respectively, of the cycles represented by the triggering hot-wire time series. A value $N = 7$ indicates that the structure interval is ± 3.5 ms. The educed coherent vorticity using this technique is shown in Fig. 4.

In summary, a new conditional-sampling/phase-averaging method is introduced for the eduction of the natural large-scale coherent structures. Constant threshold level methods, which give rather satisfactory results in the eduction of the coherent structures in excited flows, fail in the unexcited case of the complex flows. The life cycle method described in this paper offers a good way of educing the natural coherent structures in highly complex flows in which a number of modes are present. It is named the life cycle method because the conditional sampling and phase-averaging technique is based on the coherent structure's life time, which is the period between its birth and destruction.[7]

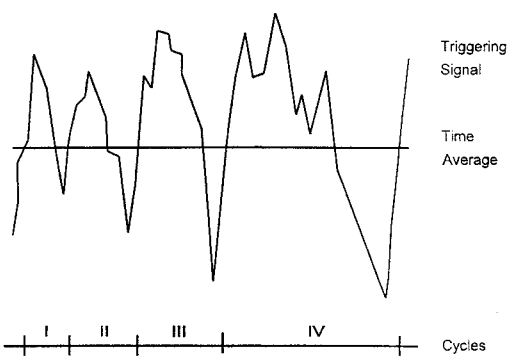

Fig. 1 Cycle definition.